Springer

KSME

Journal of Mechanical Science and Technology 26 (3) (2012) 671~680
www.springerlink.com/content/1738-494x
DOI 10.1007/s12206-011-1228-8

The effect of bending loads on the dynamic behaviors of a rolling guide †

James Shih-Shyn Wu[1,*], Jyh-Cheng Chang[2], Gent-An Tsai[1], Ching-Yuan Lin[3] and Feng-Ming Ou[3]

[1]*Institute of Mechanical Engineering, National Chung-Hsing University, Taichung, Taiwan, ROC*
[2]*Department of Automation Engineering, Nan Kai University of Technology, Nantou, Taiwan, ROC*
[3]*Mechanical and systems Research Laboratories, Industrial Technology Research Institute, Taichung, Taiwan, ROC*

(Manuscript Received January 17, 2011; Revised September 11, 2011; Accepted November 7, 2011)

Abstract

Dynamic behaviors of ball-type contact surfaces under unbalanced bending loads are studied using point-to-point analysis, three-dimensional finite element simulation based on the Hertz Contact Theory, and a modal test. Results derived from these models are very similar but the Finite Element Model provides the best results since it allows for more elements of study, such as the steel ball, carriage, rail etc. In the study, results also show that frequencies vary slightly, but there is an obvious change in shapes. Therefore, the contact stiffness in simulations must be properly selected with the conclusion that different external loadings may affect the dynamic characteristics of such structures significantly.

Keywords: Linear guide; Hertz contact theory; Contact stiffness

1. Introduction

Growth of demand for precision machinery technology in the field of modern science and industry is fast. To achieve high-speed and precise positioning, it is important to understand the mechanical behaviors of such a mechanism. Ball-type linear guideways are now widely used in the drive system because of low friction. In the ball-type linear guideway, force transferred between the carriage and rail is performed via balls. During the analysis of static and dynamic behaviors, a linear spring element is generally used to simulate the mechanical behavior of balls. During implementation, a guideway is usually pre-stressed between the balls and the carriage/rail. If the guideway is under uniform downward loads only, deformations for each ball are identical and the normal stiffness (Kn) adopted in the Hertz Contact Theory is also assumed to be identical. Because of the symmetry of the system, each mode shape, i.e. f_{RYL} (f_Y), f_{PVL} (f_P), f_{PVH} (f_V) or f_{RYH} (f_R), is related to one parameter only. However, once the bending moments are added, loadings in balls are not symmetrical and the K_n becomes unequal. Mode shapes f_{RYL} (f_R .+ f_Y), f_{PVL} ($f_P + f_V$), f_{PVH} ($f_P + f_V$) and f_{RYH} (f_R .+ f_Y) become relative to two parameters each (see following derivations in this report). Therefore, in a guideway the influence of these moments upon dynamic behavior is worthy of study here.

In the past, there have been numerous studies using Hertz Contact Theory. For example, Lynagh [1] and Hernot [2] separately discussed the vibration and stiffness matrix of ball bearings via nonlinear relationships from the Hertz Contact Theory. Pimsarn and Kazerounian [3] also put forward the theory of PISE (pseudo-interference stiffness estimation) based on Hertz's theory, which can be used to rapidly obtain gear stiffness. In terms of the study of ball-type linear guideways, Ohta and Hayashi used an energy balance method to analyze the lower rolling, yawing, pitching, vertical and higher rolling of the carriage, as well as natural vibration frequency of first/second/third flexural, in combination with Lagrange's Equation and the finite element models [4, 5]. Wu and Chang [6] studied dynamic behaviors between the balls and the carriage/rail using a three-dimensional surface-to-surface Hertz Contact Finite Element Model, and verifying with experiments they found that the finite element model was more accurate than the generally used one-dimensional and two-dimensional point-to-point contact simulations. In previous works, we only considered the dynamic behaviors of a single linear guideway in absence of external forces [6]. Recently, Yi [7] investigated the dynamic properties of the LM Guide System, by using the equivalent stiffness of the Hertz Contact Model.

Our current work studied the changes of contact interface of balls due to the external moment loadings applied to the slide block, and further explored the impact effect of such moments to understand the dynamic characteristics of a linear guideway. Here, the simulation of a contact element algorithm from our

† This paper was recommended for publication in revised form by Editor Yeon June Kang

*Corresponding author. Tel.: +886 4 23926763, Fax.: +886 4 22877170
E-mail address: sswu@dragon.nchu.edu.tw

previous work [6] was applied to the contact interface of balls to study the nonlinear characteristics. In the study, first the normal stiffness of one-dimensional point-to-point contact was calculated and vibration frequencies were derived to discuss the differences from the combined energy balance from Lagrange's Equation. With a view of the contact between the ball and the carriage/rail, Hertz's interface mode initiated by our previous work was used to derive the interface stiffness in all contact components to obtain the dynamic behaviors of a linear guideway under bending loads. Then, the finite element method was used to simulate such a ball-type linear guideway. Discussion is provided regarding the difference in frequencies and modal shapes between various models compared with experiments, and the effects of dynamic characteristics are shown by drawing up various modal patterns in the last part of this report.

2. Contact stiffness of rolling interface

In Hertz's Contact Theory it is assumed that the relationship between the applied load and deformation at the contact point is nonlinear when two objects come into contact (Johnson [8]). So, for a linear guideway mechanism, the deformation of the groove will become greater with the increase in the applied load on the rolling ball and hence the contact stiffness of the interface also rises. Thus, the dynamic behavior of the linear guideway is presented with more complicated phases. Therefore, in order to understand the correct dynamic characteristics of a linear guideway, the contact stiffness must be properly defined, referring to Johnson [8] and Goldsmith [9]. The algorithm for calculating the stiffness based on Hertz's Contact Theory is described in the following.

Fig. 1 shows the contact relationship between the deformation and the applied load. When a compressive load F is applied, the contact area of these two objects deforms a value of α in the normal direction and presents an elliptic shape. The configuration of deformation can be expressed as

$$F = k_h \alpha^{3/2} \tag{1}$$

$$k_h = \frac{4}{3}\frac{q_k}{(\delta_1+\delta_2)\sqrt{A+B}} \tag{2}$$

$$\delta_i = \frac{1-\mu_i}{\pi E_i} \tag{3}$$

$$a = q_a \sqrt[3]{\frac{3F(\delta_1+\delta_2)}{4(A+B)}} \tag{4}$$

$$b = q_b \sqrt[3]{\frac{3F(\delta_1+\delta_2)}{4(A+B)}} \tag{5}$$

where α is the normal deformation of the contact area, K_h is the constant and δ_i, δ_1, δ_2 are material properties of Hertz's Contact Theory, E is Young's Modulus, μ is Poisson's Ratio of Materials, and a is the semi-major and b is the semi-minor of the contact ellipse. Constants A, B, q_a, q_b, and q_k are taken from the surface geometry (Goldsmith [9]). In this study,

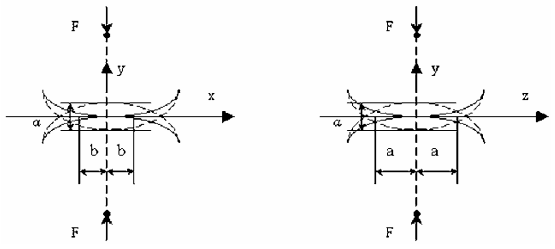

(a) Front view (b) Side view

Fig. 1. Loadings and deformed shapes at contact boundary.

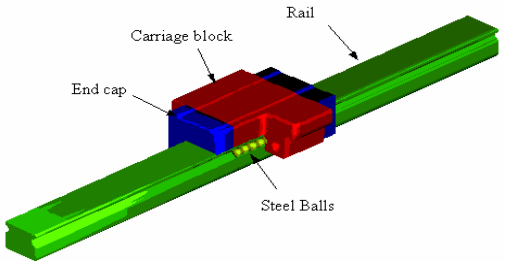

(a)

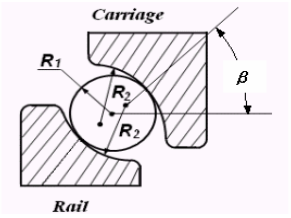

(b)

Fig. 2. (a) Schematic of a linear guide system; (b) geometry of the rolling ball in contact with rail and carriage.

the configuration of contact in a linear guideway is simplified with a sphere of radius R_1 and a cylindrical cup of radius R_2 (see Fig. 2). Therefore, we have

$$A = \frac{1}{2}\left(\frac{1}{R_1} - \frac{1}{R_2}\right) \tag{6}$$

$$B = \frac{1}{2R_1}. \tag{7}$$

From Eq. (1), the normal stiffness can be obtained as

$$K_n = \frac{dF}{d\alpha} = \frac{3}{2}k_h \alpha^{(1/2)}. \tag{8}$$

3. Analytical approach

3.1 Natural frequency of the rigid-body carriage

In mathematical modeling, the linear guideway is considered as a spring mass system in which the rail and carriage are modeled as rigid bodies and connected with a series of spring elements with adequate spring stiffness. The coordinate system and vibration mode of the carriage are illustrated in Fig.

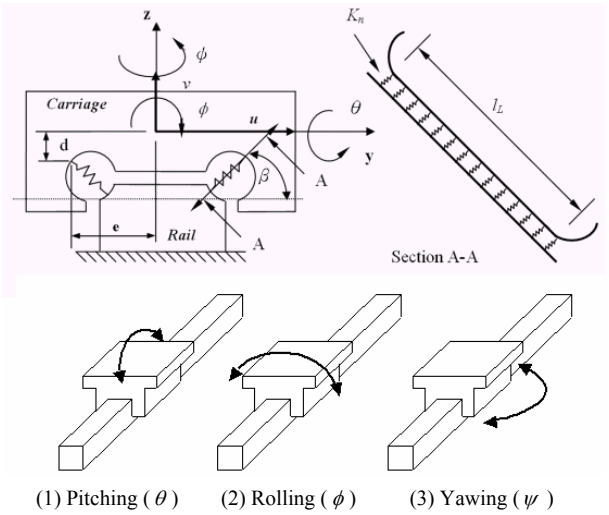

Fig. 3. Coordinate system describing the motion mode of carriage, in which β is the contact angle, u and v are the displacements in the y-axis and z-axis, respectively. ϕ, θ and ψ are the angular displacements about the x-axis, y-axis and z-axis, which are termed pitching, rolling and yawing motion, respectively (NSK Ltd.).

3(a), where the origin of the coordinate is located at the mass center of the carriage block and the sliding direction of the carriage block is along the x-axis, β is the contact angle of the rolling ball, d and e are the distances from the contact point between the rolling ball and carriage to the x-y plane and the x-z plane, respectively, and l_L is the length of the loading zone of the balls. For such a spring mass system, we can define the vibration mode associated with the motion degrees of freedom. As shown in Fig. 3(b) (NSK [10]), the main motion in a vertical direction is called the vertical vibration mode, the rocking motion θ about the y-axis is called the pitching vibration mode, the rocking motion ψ about the z-axis is called the yawing vibration mode and the rocking motion ϕ about the x-axis is called the rolling vibration mode.

Since the linear spring is perpendicular to the x-axis, the displacement along the x-axis is not considered. In addition, in Fig. 3(a), a spring element is introduced at the location of the ball bearing and quantified with the stiffness K_n in the normal contact direction, which is the contact stiffness of the rolling ball against the raceway groove and is determined based on the Hertzian Theory. Using this simplified model and following Ohta and Hayashi [5], the governing equations of the five degrees of a freedom model were derived in terms of the application of Lagrange's approach to the potential energy of the linear guideway system.

The natural frequencies of the vibration of the carriage are shown at the conclusion of our paper (for details, see Appendix).

$$f_Y = \frac{\omega_{11}}{2\pi} = \frac{1}{2\pi}\sqrt{\frac{2K_n\cos^2\beta}{J_z}\sum_{i=1}^{Z_L} l_i^2} \tag{9}$$

$$f_P = \frac{\omega_{12}}{2\pi} = \frac{1}{2\pi}\sqrt{\frac{2K_n\sin^2\beta}{J_Y}\sum_{i=1}^{Z_L} l_i^2} \tag{10}$$

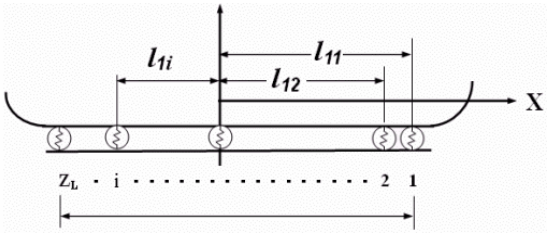

Fig. 4. Location of the ith ball or spring element at right row or left row of raceways, which is measured from y-z plane.

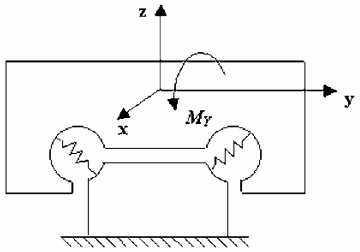

Fig. 5. Modeling of the rolling contact by using a spring element with normal stiffness K_n.

$$f_V = \frac{\omega_{13}}{2\pi} = \frac{1}{2\pi}\sqrt{\frac{2Z_L K_n \sin^2\beta}{M}} \tag{11}$$

$$f_R = \frac{\omega_{14}}{2\pi} = \frac{1}{2\pi}\sqrt{\frac{c_{13}M + c_{11}J_x}{M\ J_x}} \tag{12}$$

where

$$l_{1i}, l_{2i} = \left(\frac{Z_L - 2i + 1}{2Z_L}\right) l_L = l_i \tag{13}$$

$$\left.\begin{aligned} c_{11} &= 2Z_L K_n \cos^2\beta \\ c_{12} &= -2Z_L K_n d\cos^2\beta - 2Z_L K_n e\sin\beta\cos\beta \\ c_{13} &= 2Z_L K_n d^2\cos^2\beta + 4Z_L K_n de\sin\beta\cos\beta + 2Z_L K_n e^2\sin^2\beta \end{aligned}\right\}. \tag{14}$$

In Eqs. (9)-(14), M is the mass of the carriage, Z_L is the average number of balls existing at the load zone, J_x, J_y and J_z are the moments of inertia about the x-axis, y-axis and z-axis, respectively, l_{1i}, l_{2i}, l_i are the locations of the ith ball or spring element measured from the y-z plane, and subscripts 1 and 2 represent the left and right rows of raceways, respectively (shown in Fig. 4).

3.2 Moment effects on natural frequency of the rigid-body carriage

Moments are usually produced by unbalanced loads distributed on the carriage. Under such a condition, rolling balls on both sides of the raceway may experience different extents of contact loading, which in turn induce different normal stiffness K_n at the rolling interface and hence affect the vibration characteristics of the guideway. To consider the moment effect on the natural frequency of the rigid-body carriage, we

derived an equilibrium equation for the carriage subjected to moment loading cases, represented by M_Y here. In Fig. 5, the moment is applied on the carriage block along a y-axis direction, and the natural frequencies of the vibrations of the carriage are stated later in the paper (for details, see Appendix).

$$f_{RYL} = \frac{\omega_{21}}{2\pi} \tag{15}$$

$$f_{PVL} = \frac{\omega_{22}}{2\pi} \tag{16}$$

$$f_{PVH} = \frac{\omega_{23}}{2\pi} \tag{17}$$

$$f_{RYH} = \frac{\omega_{24}}{2\pi} \tag{18}$$

where

$$\omega_{21,24}^2 = \frac{-a_1 \mp \sqrt{a_1^{\,2} - 4a_2 M J_x J_z}}{2MJ_x J_z} \tag{19}$$

$$\omega_{22,23}^2 = \frac{c_{29}M + c_{27}J_y \mp \sqrt{(c_{29}M + c_{27}J_y)^2 - 4MJ_y(c_{27}c_{29} - c_{228}^2)}}{2MJ_y} \tag{20}$$

$$\left.\begin{aligned} a_1 &= -(c_{21}J_xJ_z + c_{23}MJ_z + c_{25}MJ_x) \\ a_2 &= -(c_{24}^{\,2}J_x + c_{26}^{\,2}M + c_{22}^{\,2}J_z - c_{23}c_{25}M - c_{21}c_{25}J_x - c_{21}c_{23}J_z) \\ a_3 &= -(c_{21}c_{23}c_{25} + 2c_{22}c_{24}c_{26} - c_{24}^{\,2}c_{23} - c_{26}^{\,2}c_{21} - c_{22}^{\,2}c_{25}) \end{aligned}\right\} \tag{21}$$

$$\left.\begin{aligned} c_{21} &= \sum_{i=1}^{Z_L} K_{ni}\{2\cos^2\beta\} \\ c_{22} &= \sum_{i=1}^{Z_L} K_{ni}\{-2d\cos^2\beta - 2e\sin\beta\cos\beta\} \\ c_{23} &= \sum_{i=1}^{Z_L} K_{ni}\{2d^2\cos^2\beta + 4de\sin\beta\cos\beta + 2e^2\sin^2\beta\} \\ c_{24} &= \sum_{i=1}^{Z_L} K_{ni}\{2l_i\cos^2\beta\} \\ c_{25} &= \sum_{i=1}^{Z_L} K_{ni}\{2l_i^2\cos^2\beta\} \\ c_{26} &= \sum_{i=1}^{Z_L} K_{ni}\{-2dl_i\cos^2\beta - 2el_i\sin\beta\cos\beta\} \end{aligned}\right\} \tag{22}$$

$$\left.\begin{aligned} c_{27} &= \sum_{i=1}^{Z_L} K_{ni}\{2\sin^2\beta\} \\ c_{28} &= \sum_{i=1}^{Z_L} K_{ni}\{-2l_i\sin^2\beta\} \\ c_{29} &= \sum_{i=1}^{Z_L} K_{ni}\{2l_i^2\sin^2\beta\} \end{aligned}\right\}. \tag{23}$$

In Eqs. (22) and (23), the normal stiffness K_{ni} is the ith ball or spring element existing at load zone.

4. Finite element approach

Apart from the analytical approach, factors influencing the dynamics of a linear guide system are considered in this study. All components in the linear guideway are assumed to be elastic and the contact status coming from the elastic contact deformation of the groove of the raceway and carriage is considered as a three- dimensional surface mode.

Table 1. Specifications of the linear guide system.

Carriage length	65.9 mm
Carriage width	59 mm
Carriage height	22 mm
Rail length	500 mm
Rail width	20 mm
Rail height	15.5 mm
Diameter of steel ball	4.763 mm
Total number of balls	50
Number of row	2
Contact angle β	45°
Load zone length l_L	43 mm
Mass of carriage, M	0.313kg
Inertial moment about the x-axis, J_X	9.938 x 10^{-5} kg-m^2
Inertial moment about the y-axis, J_Y	6.136 x 10^{-5} kg- m^2
Inertial moment about the z-axis , J_Z	1.394 x 10^{-4} kg- m^2
d	7.37 mm
e	10.3 mm

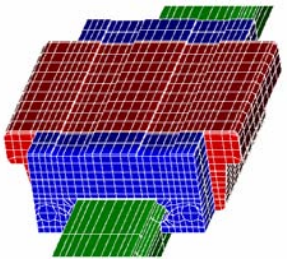

Fig. 6. The finite element model of linear guide system, including rail, carriage, rolling ball and end caps.

Fig. 6 shows the 3-D finite element model of a linear guideway mechanism with the specifications listed in Table 1. The contact configuration within this mechanism is depicted in Fig. 7, in which the two rows of balls roll between the carriage and raceway. Each ball is meshed with an adequate number of brick elements, having a total mass equivalent to the ball mass. In order to model the contact characteristic of the rolling interface, the contact elements with zero thicknesses are applied to the upper and lower sides of each ball. The stiffnesses K_n of such contact elements are calculated according to the formulae described in section 2. In the finite element simulation, hexahedron solid elements are adopted. The carriage block, with end caps at both sides, is modeled with 3830 elements and 480 elements, respectively, while the rail is modeled using 2158 elements. As a whole, there are 6648 elements and 9396 nodes applied in this system for finite element analysis. The material of the components, such as the

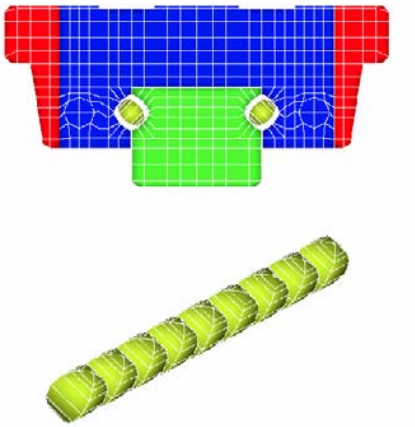

Fig. 7. Finite element mesh of transverse cross section, showing the contact configuration between carriage and rail, in which each rolling ball is meshed using brick elements with a mass equivalent to the ball.

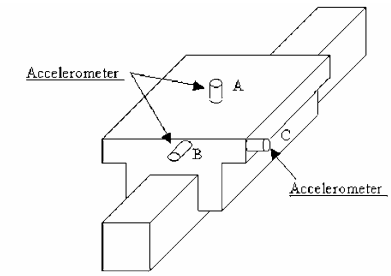

Fig. 8. Configuration of modal experiment and accelerometer positions (A, B, C) for measuring various vibration modes.

ball, carriage and rail, is steel with the properties of Young's Modulus $E = 206$GPa, and Poisson's Ratio $\nu = 0.30$, density $\rho = 7800$ Kg/m^3, while the end caps have properties of $E = 3.57$GPa, and Poisson's Ratio $\nu = 0.30$, density $\rho = 1400$ Kg/m^3. Again, the stiffness K_C was assigned between the carriage block and the ball bearing, and the stiffness K_R between the ball bearing and rail. For simplification in computation, all contact surfaces were assumed to have the same values, namely, $K_C = K_R = K_n$.

5. Experimental measurements

Here, modal tests were conducted to measure the vibration characteristics of workshop-supplied guideways. Fig. 8 shows the experimental configuration for measuring the vibration of the linear guide system. An accelerometer was attached to different positions on the carriage. Accelerometer A was used to measure the vertical mode of the carriage, accelerometer B measured the pitching mode and accelerometer C measured the yawing and rolling modes. To investigate the preload effect, two linear guideways with different moments in the y-axis direction were employed during experiments (refer to Fig. 5). In these experiments, the vibration amplitudes were recorded and stored in a digital spectrum analyzer after hammering the carriage along the measuring direction.

The vibration spectra corresponding to the three measuring

Table 2. Normal stiffness K_n of the linear guide system.

ith ball	$M_Y = 0$	M_Y =1.45 N-m	M_Y = 2.90 N-m	M_Y = 4.35 N-m
K_{n1}	17.8 x 10^6 N/m	15.7 x 10^6 N/m	12.9 x 10^6 N/m	7.6 x 10^6 N/m
K_{n2}	17.8 x 10^6 N/m	16.3 x 10^6 N/m	14.5 x 10^6 N/m	12.0 x 10^6 N/m
K_{n3}	17.8 x 10^6 N/m	16.8 x 10^6 N/m	15.7 x 10^6 N/m	14.5 x 10^6 N/m
K_{n4}	17.8 x 10^6 N/m	17.3 x 10^6 N/m	16.8 x 10^6 N/m	16.3 x 10^6 N/m
K_{n5}	17.8 x 10^6 N/m	17.8 x 10^6 N/m	17.8 x 10^6 N/m	17.8 x 10^6 N/m
K_{n6}	17.8 x 10^6 N/m	18.2 x 10^6 N/m	18.6 x 10^6 N/m	19.0 x 10^6 N/m
K_{n7}	17.8 x 10^6 N/m	18.6 x 10^6 N/m	19.4 x 10^6 N/m	20.2 x 10^6 N/m
K_{n8}	17.8 x 10^6 N/m	19.0 x 10^6 N/m	20.2 x 10^6 N/m	21.2 x 10^6 N/m
K_{n9}	17.8 x 10^6 N/m	19.4 x 10^6 N/m	20.8 x 10^6 N/m	22.1 x 10^6 N/m

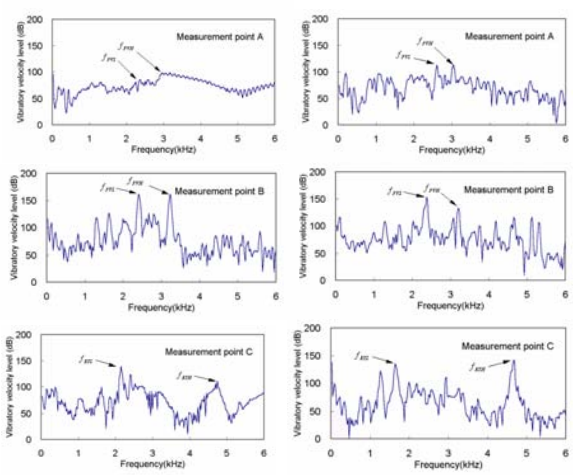

(a) M_Y =1.45 N-m (b) M_Y =2.90 N-m

Fig. 9. Vibration spectra of linear guideway.

points A, B and C are depicted in Fig. 9. The main peaks of each measurement point were generalized to obtain the fundamental frequency, and the associated vibration modes can be identified by comparing them to the mode shapes predicted by the finite element approach.

6. Results and discussions

6.1 Natural frequency of carriage

The natural frequencies, f_Y, f_P, f_V and f_R, corresponding to different vibration modes were calculated by substituting the constants in Tables 1 and 2 into the mathematical models described previously. The results obtained from an analytical approach and finite element simulation are listed in Table 3 and depicted in Fig. 10 for comparison. It can be seen from Fig. 10 that the 1-D contact model predicts the natural frequencies to be higher than the frequency corresponding to the finite element contact model. This can be easily realized because the ball, carriage block and rail were all assumed to be rigid and only the deformation of the contact interface was considered in the analytical calculations.

Comparison of results obtained from finite element simulation and analytical calculations also shows that the 1-D point-

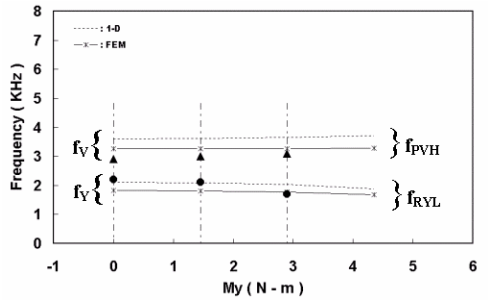

(a) Yawing and vertical modes

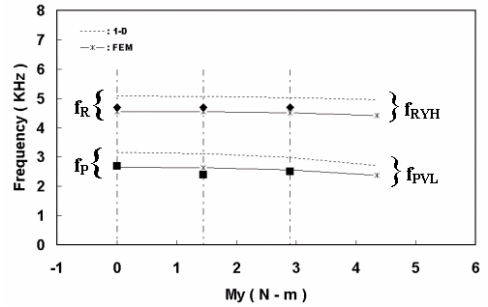

(b) Pitching and rolling modes

Fig. 10. Comparisons of the natural frequencies of rolling guides with different preloads. Results are obtained from numerical predictions and experimental measurements, respectively, in which the bold symbols ●▲■◆ represent experimentally measured values.

to-point contact model predicts a higher frequency than the finite element method using a surface contact model. This is due to the fact that the finite element model was assumed to be an elastic structure and hence possesses a lower structural stiffness than a rigid one in an analytical approach. Because of this, the surface-to-surface contact mode with Hertzian contact stiffness demonstrates the contact characteristic of the rolling contact interface in a realistic way. The predicted finite element vibration modes of the linear guide system corresponding to each frequency are further depicted in Fig. 11. This figure clearly shows the variety of mode shapes in a linear guide system, which includes the mode shape of yawing, pitching, vertical and rolling vibration. The frequencies of these modes are in the sequence: yawing < pitching < vertical < rolling.

6.2 Effect of moments

The natural frequencies, f_{RYL}, f_{PVL}, f_{PVH} and f_{RYH}, corresponding to different vibration modes were calculated by substituting the constants in Tables 1 and 2 into the mathematical models. The natural frequencies of the carriage block, estimated by the proposed analytical method and finite element approach, are listed in Table 3. Both approaches predicted the same vibration modes. The vibration modes of the linear guide system corresponding to each frequency are further depicted in Fig. 11.

To investigate the effect of the loading conditions on the vi-

Table 3. Natural frequencies at different vibration mode of a linear guide system.

(a) M_Y = 0 N-m

Degree of freedom	Mode	Frequency (kHz)		
		Experimental measurement	FEM	1-D Point-to-point contact model
ψ	Yawing	2.2(f_Y)	1.82(f_Y)	2.10(f_Y)
θ	Pitching	2.7(f_P)	2.65(f_P)	3.16(f_P)
v	Vertical	2.9(f_V)	3.26(f_V)	3.60(f_V)
ϕ ,u	Rolling	4.7(f_R)	4.55(f_R)	5.08(f_R)

(b) M_Y =1.45 N-m

Degree of freedom	Mode	Frequency (kHz)		
		Experimental measurement	FEM	1-D Point-to-point contact model
ψ, ϕ ,u	Lower rolling - yawing	2.1(f_{RYL})	1.81(f_{RYL})	2.08(f_{RYL})
θ,v	Lower Pitching - vertical	2.4(f_{PVL})	2.63(f_{PVL})	3.12(f_{PVL})
v ,θ	Higher Pitching - vertical	3.0(f_{PVH})	3.26(f_{PVH})	3.61(f_{PVH})
ϕ ,u,ψ	Higher rolling - yawing	4.7(f_{RYH})	4.54(f_{RYH})	5.06(f_{RYH})

(c) M_Y =2.90 N-m

Degree of freedom	Mode	Frequency (kHz)		
		Experimental measurement	FEM	1-D Point-to-point contact model
ψ, ϕ ,u	Lower rolling - yawing	1.7(f_{RYL})	1.78(f_{RYL})	2.03(f_{RYL})
θ,v	Lower Pitching - vertical	2.5(f_{PVL})	2.56(f_{PVL})	2.99(f_{PVL})
v ,θ	Higher Pitching - vertical	3.1(f_{PVH})	3.27(f_{PVH})	3.66(f_{PVH})
ϕ ,u,ψ	Higher rolling - yawing	4.7(f_{RYH})	4.51(f_{RYH})	5.03(f_{RYH})

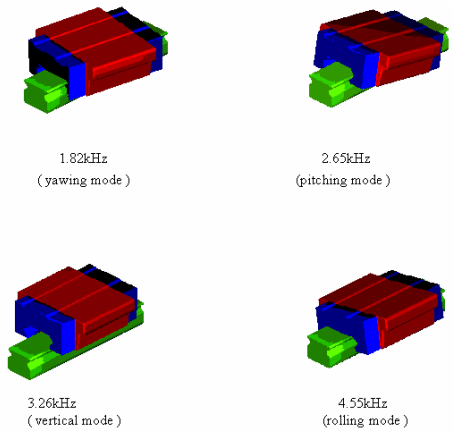

Fig. 11. Mode shapes of carriage at different vibration frequencies, predicted by finite element analysis. Flow chart for the correction of the roll forming process design.

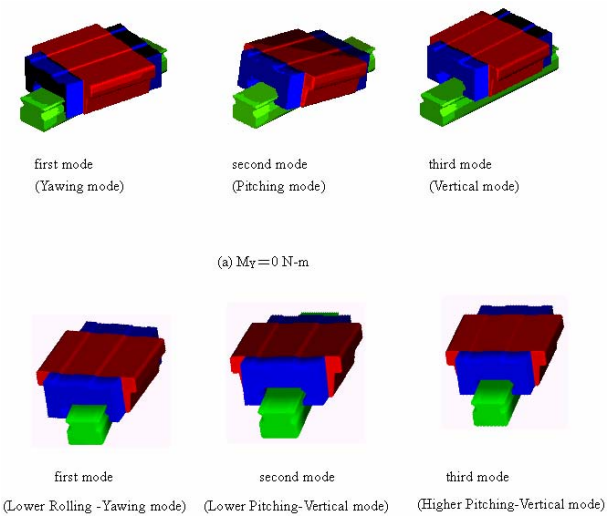

Fig. 12. Vibration modes under different loading conditions Flow chart for the correction of the roll forming process design.

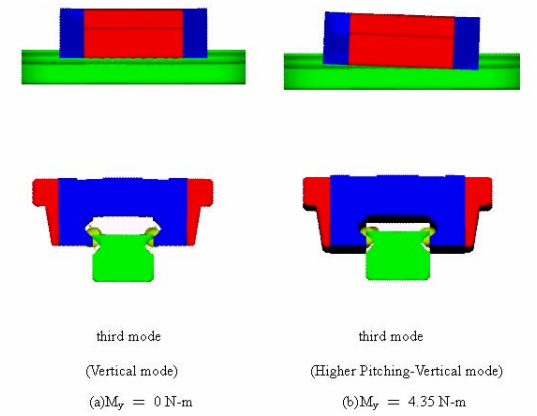

Fig. 13. Moment effect on vibration modes of linear guide system.

bration mode, some special modes are depicted in Fig. 12 for comparison. It was found that when the carriage block is free of moment, it will vibrate at natural frequencies f_Y, f_P, f_V and f_R. However, if a moment M_Y is applied to the carriage block, it will vibrate at frequencies f_{RYL}, f_{PVL}, f_{PVH} and f_{RYH}. As observed in Fig. 12, the carriage block behaves with different mode shapes under the absence of moment or in the event of moment. Take the second and third modes, for example, when the carriage block is not subjected to moment, the natural frequencies f_P and f_V of the carriage block are only related to the variable θ rotating about the y-axis and variable v shifting along the z-axis, respectively. In cases where the carriage block is subjected to moment, the natural frequencies f_{PVL} and f_{PVH} of the carriage block are obviously related to both displacement components of θ and v.

To manifest such differences in vibration modes more clearly, we depicted the mode shapes in different views. It can be seen from Fig. 13 that the third mode in the z-direction was induced by the moment loading and resulted in a vibration mode with pitching and vertical motion, instead of the only vertical mode occurring under the absence of moment; while the front and top views of the third mode show that the dominating vibration mode will change from vertical motion into a combination of pitching and vertical motion. This vertical motion is contributed to by the displacement component v that is initiated by moment loading.

Based on findings from this study, some other factors affecting the dynamic behavior of the guide can be presumed. For example, the moment loading effect may arise due to an unevenly distributed load on the carriage or a load applied from a different direction, which is expected to cause different contact forces acting on the rolling balls. This may further generate various contact stiffnesses at different rolling interfaces, especially at each row of ball grooves and hence enable the guide to exhibit unexpected vibration characteristics, including mode shapes and frequencies. Such an effect was demonstrated by the currently proposed finite element approach. The final results obtained from this study further suggest that the load acting on the carriage should be held adequately in place to maintain the rolling guideway's operation with good dynamic performance.

7. Conclusions

This study focused on the investigation of unbalanced bending effects on the dynamic behaviors of a rolling guideway. Some conclusions can be summarized from the experimental results, the analytical and the finite element approach as follows:

(1) We can obtain suitable stiffness using the nonlinearity of the Hertzian Contact Theory, according to the contact geometry between the rolling ball and raceway of the carriage block or linear guideway system.

(2) When the bending moment is applied to the carriage, the contact stiffness at each rolling contact site varies with the contact force of the rolling ball, which is due to unevenly distributed loading on the carriage of the guideway system.

(3) When the carriage block is not subjected to loadings like a bending moment, some modal frequencies, such as rolling, yawing, pitching, and vertical frequencies, are only related to one motion degree of freedom. However, when the carriage is subjected to loading moments from different directions, the rolling guideway behaves in a vibration mode, coupled by multi-degrees of freedom. In this paper, the vibration behavior includes different mode shapes at (a) a lower rolling-yawing natural frequency, (b) a higher rolling-yawing natural frequency, (c) a lower pitching-vertical natural frequency, and (d) a higher pitching-vertical natural frequency.

(4) According to the Hertzian Contact Theory, the contact stiffness between the rolling ball and raceway presents a nonlinear changing tendency along with the changing of contact force between the two objects in the linear rolling guideway system. Therefore, this study first used static balance to analyze the contact force between each rolling ball and the carriage block or raceway, and then calculated the contact stiff-

ness between them using the nonlinearity nature of the Hertzian Contact Theory. Finally, they were led into the finite elements to analyze the modal of the entire system.

(5) This paper shows that, the results predicted by a finite element approach using a surface contact model are in good agreement with the experimental measurements, when compared with the analytical approach using a linear spring element. It is believed that the proposed method, as based on the Hertzian Contact Theory, can provide a more realistic way for modeling a rolling contact interface.

Acknowledgment

This study was supported by the Mechanical and systems Research Laboratories of Industrial Technology Research Institute.

References

[1] N. Lynagh, H. Rahnejat, M. Erahimi and R. Aini, Bearing induced vibration in precision high speed routing spindle, *International Journal of Machine Tools & Manufacture*, 40 (2000) 561-577.

[2] X. Hernot, M. Sartor and J. Guillot, Calculation of the stiffness matrix of angular contact ball bearings by using the analytical approach, *Journal of Mechanical Design*, 122 (March) (2000) 83-90.

[3] M. Pimsarn and K. Kazerounian, Efficient evaluation of spur gear tooth mesh load using pseudo-interference stiffness estimation method, *Mechanism and Machine Theory*, 37 (2002) 769-786.

[4] H. Ohta, Sound of guideway type recirculating linear ball bearings, *Transactions of the ASME Journal of Tribology*, 121 (1999) 678-685.

[5] H. Ohta and E. Hayashi, Vibration of linear guideway type recirculating linear ball bearings, *Journal of Sound and Vibration*, 235 (5) (2000) 847-861.

[6] S. S. Wu, J. C. Chang and J. P. Hung, The effect of contact interface on dynamic characteristics of composite structures, *Mathematics and Computers in Simulation*, 74 (6) (2007) 454-467.

[7] Y. S. Yi, Y. Y. Kim, J. S. Choi, J. Yoo, D. J. Lee, S. W. Lee and S. J. Lee, Dynamic analysis of a linear motion guide having rolling elements for precision positioning devices, *Journal of Mechanical Science and Technology*, 22 (2008) 50-60.

[8] K. J. Johnson, Contact *mechanics*, Cambridge University Press (1985).

[9] W. Goldsmith, *Impact-the theory and physical behavior of colliding solids*, Edward Arnold Ltd. (1960).

[10] NSK., Selection *guide to NSK linear guides,* NSK Ltd.

Appendix

Using the notation used in section 3.1 and 3.2, the total kinetic energy E_K can be expressed as:

$$E_K = \frac{1}{2}M\,\dot{u}^2 + \frac{1}{2}M\,\dot{v}^2 + \frac{1}{2}J_x\,\dot{\phi}^2 + \frac{1}{2}J_y\,\dot{\theta}^2 + \frac{1}{2}J_z\,\dot{\psi}^2 . \quad \text{(A1)}$$

The potential energy E_p is given by:

$$E_P = \sum_{i=1}^{Z_L}\frac{1}{2}K_{ni}(\delta_{1i}^2 + \delta_{2i}^2) \quad \text{(A2)}$$

$$E_P = \sum_{i=1}^{Z_L}\frac{1}{2}K_{ni}[\{(u - d\phi + l_i\psi)\cos\beta + (-v - e\phi + l_i\theta)\sin\beta\}^2 + \{-(u - d\phi + l_i\psi)\cos\beta + (-v + e\phi + l_i\theta)\sin\beta\}^2] \quad \text{(A3)}$$

where

$$l_{1i}, l_{2i} = (\frac{Z_L - 2i + 1}{2Z_L})l_L = l_i . \quad \text{(A4)}$$

In the above equations, E_P is the potential energy of normal spring, δ_{1i} and δ_{2i} are the displacement of the ith ball existing at the left and right load zone, respectively, Z_L is the average number of balls existing at the load zone, l_{1i}, l_{2i}, l_i are the location of the ith ball or spring element measured from y-z plane, and the subscript 1 and 2 represent the left and right row of raceways, respectively (shown in Fig. 4).

Applying the Lagrange's approach to Eqs. (A1) and (A2), we can derive the motion equation with respect to different degree of freedom.

$$M\ddot{u} + \sum_{i=1}^{Z_L}K_{ni}\{2\cos^2\beta\}u + \sum_{i=1}^{Z_L}K_{ni}\{-2d\cos^2\beta - 2e\sin\beta\cos\beta\}\phi + \sum_{i=1}^{Z_L}K_{ni}\{2l_i\cos^2\beta\}\psi = 0 \quad \text{(A5)}$$

$$M\ddot{v} + \sum_{i=1}^{Z_L}K_{ni}\{2\sin^2\beta\}v + \sum_{i=1}^{Z_L}K_{ni}\{-2l_i\sin^2\beta\}\theta = 0 \quad \text{(A6)}$$

$$J_x\ddot{\phi} + \sum_{i=1}^{Z_L}K_{ni}\{-2d\cos^2\beta - 2e\sin\beta\cos\beta\}u + \sum_{i=1}^{Z_L}K_{ni}\{2d^2\cos^2\beta + 4de\sin\beta\cos\beta + 2e^2\sin^2\beta\}\phi + \sum_{i=1}^{Z_L}K_{ni}\{-2d\,l_i\cos^2\beta - 2el_i\sin\beta\cos\beta\}\psi = 0 \quad \text{(A7)}$$

$$J_y\ddot{\theta} + \sum_{i=1}^{Z_L}K_{ni}\{2l_i^2\sin^2\beta\}\theta + \sum_{i=1}^{Z_L}K_{ni}\{-2l_i\sin^2\beta\}v = 0 \quad \text{(A8)}$$

$$J_z\ddot{\psi} + \sum_{i=1}^{Z_L}K_{ni}\{2l_i^2\cos^2\beta\}\psi + \sum_{i=1}^{Z_L}K_{ni}\{-2d\,l_i\cos^2\beta - 2el_i\sin\beta\cos\beta\}\phi + \sum_{i=1}^{Z_L}K_{ni}\{2l_i\cos^2\beta\}u = 0 \quad \text{(A9)}$$

In the above equations, K_{ni} is the stiffness of the ith ball existing at the load zone, which is determined base on Hertzian theory, M is the mass of the carriage, J_x、J_y and J_z are the moments of inertia about the x-axis, y-axis and z-axis, respectively.

Since Eqs. (A5), (A7) and (A9), the displacement u along the y-axis, the angular displacement ϕ about x-axis and the angular displacement ψ about z-axis are mutually coupled, we may assume solution is of the form

$$\left.\begin{aligned} u &= Ue^{j\omega t} \\ \phi &= \Phi e^{j\omega t} \\ \psi &= \Psi e^{j\omega t} \end{aligned}\right\} \tag{A10}$$

$$\begin{bmatrix} c_{21}-M\omega^2 & c_{22} & c_{24} \\ c_{22} & c_{23}-J_x\omega^2 & c_{26} \\ c_{24} & c_{26} & c_{25}-J_z\omega^2 \end{bmatrix}\begin{bmatrix} U \\ \Phi \\ \Psi \end{bmatrix}=0 \tag{A11}$$

where

$$\left.\begin{aligned} c_{21} &= \sum_{i=1}^{Z_L} K_{ni}\{2\cos^2\beta\} \\ c_{22} &= \sum_{i=1}^{Z_L} K_{ni}\{-2d\cos^2\beta - 2e\sin\beta\cos\beta\} \\ c_{23} &= \sum_{i=1}^{Z_L} K_{ni}\{2d^2\cos^2\beta + 4de\sin\beta\cos\beta + 2e^2\sin^2\beta\} \\ c_{24} &= \sum_{i=1}^{Z_L} K_{ni}\{2l_i\cos^2\beta\} \\ c_{25} &= \sum_{i=1}^{Z_L} K_{ni}\{2l_i^2\cos^2\beta\} \\ c_{26} &= \sum_{i=1}^{Z_L} K_{ni}\{-2dl_i\cos^2\beta - 2el_i\sin\beta\cos\beta\} \end{aligned}\right\}. \tag{A12}$$

The three solutions ω_{20}^2, ω_{21}^2 and ω_{24}^2 ($\omega_{20}^2 < \omega_{21}^2 < \omega_{24}^2$) can be obtained by solving above Eq. (A11).

$$\omega_{20}^2 = 0 \tag{A13}$$

$$\omega_{21,24}^2 = \frac{-a_1 \mp \sqrt{a_1^{\,2} - 4a_2MJ_xJ_z}}{2MJ_xJ_z} \tag{A14}$$

where

$$\left.\begin{aligned} a_1 &= -(c_{21}J_xJ_z + c_{23}MJ_z + c_{25}MJ_x) \\ a_2 &= -(c_{24}{}^2J_x + c_{26}{}^2M + c_{22}{}^2J_z - c_{23}c_{25}M - c_{21}c_{25}J_x - c_{21}c_{23}J_z) \\ a_3 &= -(c_{21}c_{23}c_{25} + 2c_{22}c_{24}c_{26} - c_{24}{}^2c_{23} - c_{26}{}^2c_{21} - c_{22}{}^2c_{25}) \end{aligned}\right\}. \tag{A15}$$

The lowest rolling-yawing natural frequencies of the vibration of the carriage are

$$f_{RYL} = \frac{\omega_{21}}{2\pi}. \tag{A16}$$

The highest rolling-yawing natural frequencies of the vibration of the carriage are

$$f_{RYH} = \frac{\omega_{24}}{2\pi}. \tag{A17}$$

Since Eqs. (A6) and (A8), the displacement v along the z-axis is coupled with the angular displacement θ about y-axis, we may assume that the solution is of the following form:

$$\left.\begin{aligned} v &= Ve^{j\omega t} \\ \theta &= \Theta e^{j\omega t} \end{aligned}\right\} \tag{A18}$$

$$\begin{bmatrix} c_{27}-M\omega^2 & c_{28} \\ c_{28} & c_{29}-J_x\omega^2 \end{bmatrix}\begin{bmatrix} V \\ \Theta \end{bmatrix}=0 \tag{A19}$$

where

$$\left.\begin{aligned} c_{27} &= \sum_{i=1}^{Z_L} K_{ni}\{2\sin^2\beta\} \\ c_{28} &= \sum_{i=1}^{Z_L} K_{ni}\{-2l_i\sin^2\beta\} \\ c_{29} &= \sum_{i=1}^{Z_L} K_{ni}\{2l_i^2\sin^2\beta\} \end{aligned}\right\}. \tag{A20}$$

Finally, the two solutions ω_{22}^2 and ω_{23}^2 ($\omega_{22}^2 < \omega_{23}^2$) can be obtained by solving above Eq. (A19).

$$\omega_{22,23}^2 = \frac{c_{29}M + c_{27}J_y \mp \sqrt{(c_{29}M + c_{27}J_y)^2 - 4MJ_y(c_{27}c_{29} - c_{28}^2)}}{2MJ_y} \tag{A21}$$

The lowest pitching-vertical natural frequencies of the vibration of the carriage are

$$f_{PVL} = \frac{\omega_{22}}{2\pi}. \tag{A22}$$

The highest pitching-vertical natural frequencies of the vibration of the carriage are

$$f_{PVH} = \frac{\omega_{23}}{2\pi}. \tag{A23}$$

If no moment M_Y is applied to the carriage block, the normal stiffness K_{ni} of the ith ball existing at load zone are equal.

$$K_{n1} = K_{n2} = \cdots\cdots = K_n \tag{A24}$$

The scalar quantities c_{24}, c_{26} and c_{28} become zero. The natural frequencies can be obtained as follows:

The yawing natural frequency of the vibration of the carriage is

$$f_Y = \frac{\omega_{11}}{2\pi} = \frac{1}{2\pi}\sqrt{\frac{2K_n\cos^2\beta}{J_z}\sum_{i=1}^{Z_L} l_i^2}. \tag{A25}$$

The pitching natural frequency of the vibration of the carriage is

$$f_P = \frac{\omega_{12}}{2\pi} = \frac{1}{2\pi}\sqrt{\frac{2K_n\sin^2\beta}{J_Y}\sum_{i=1}^{Z_L} l_i^2}. \tag{A26}$$

The vertical natural frequency of the vibration of the carriage is

$$f_V = \frac{\omega_{13}}{2\pi} = \frac{1}{2\pi}\sqrt{\frac{2Z_L K_n \sin^2\beta}{M}} \,. \tag{A27}$$

The rolling natural frequencies of the vibration of the carriage are

$$f_R = \frac{\omega_{14}}{2\pi} = \frac{1}{2\pi}\sqrt{\frac{c_{13}M + c_{11}J_x}{M\ J_x}} \tag{A28}$$

where

$$\left.\begin{aligned} c_{11} &= 2Z_L K_n \cos^2\beta \\ c_{12} &= -2Z_L K_n d\cos^2\beta - 2Z_L K_n e\sin\beta\cos\beta \\ c_{13} &= 2Z_L K_n d^2\cos^2\beta + 4Z_L K_n de\sin\beta\cos\beta + 2Z_L K_n e^2\sin^2\beta \end{aligned}\right\}. \tag{A29}$$

James Shih-Shyn Wu earned his Ph.D. degree in AME Department, University of Arizona, USA, in 1984. He has more than thirty years teaching and research experiences in engineering and is the author of one book, more than 100 engineering publications and 3 patents. Dr. Wu is the source coder of a FEM/CAD software system, FEAST. Dr. Wu took up position as the lecturer, associate professor and then professor in ME Department, NCHU. He has acted consultant to the ITRI, CSIST and cooperated with some private industrial workshops in Taiwan. He is one of the pioneers of applying porous medium theory with the finite element method to understand the micromechanical behaviors in the spine and thus, honored the International Volvo Award, Sweden in 1984. He has also honored many times by National Science Council and some society/association in Taiwan. He has been the department head, dean of engineering and president of a National University of Technology in Taiwan.